On spectral/hp simulations of heat-exchange effects in low-Mach non-stationary fluid flow

Jan Pech[1,*]

[1]Institute of Thermomechanics of the CAS, Dolejškova 1402/5, 182 00 Praha 8, Czech Republic

Abstract. Non-stationary flow of fluid, whose material properties change as influenced by heating, is the subject of this study. Model of coupled Navier-Stokes-Fourier system with temperature dependent material properties is introduced together with construction of appropriate numerical scheme. Spectral/hp element method is used as the discrete approximation of the functions in the spatial coordinates. Performance of the code implemented using Nektar++ library [1] is presented on problems of forced and natural convection around the heated cylinder.

1 Introduction

Numerical simulations of fluid flows advecting a quantity, which influences the flow field itself, are demanded across various areas of research and applications. Temperature is considered as the advected quantity in presented study, however, resulting system of equations coincides also with a wide fields of turbulent models.

We introduce results from simulations using original solver of evolutionary Navier-Stokes-Fourier system with temperature dependent material properties based on spectral/hp element approximation in space together with results from simulations of heat exchange-influenced incompressible fluid flow. Convergence in sense of temporal discretisation was verified on system which includes variable viscosity, thermal conductivity and density together with buoyancy and viscous heating. Unless we constrain to situations where compressibility can be neglected, we consider non-homogeneous divergence of velocity field as a consequence to thermal expansion, which is included naturally due to temperature dependent density. Density variation has impact not only due to the buoyancy, but also in other structural changes of the flow field, what we observe in change of measurable quantities as is the Strouhal number in the case of forced convection around the heated/cooled cylinder. Due to non-constant density, model of buoyancy is not of Boussinesque type and the solution includes hydrostatic pressure, what has to be taken into account in setting the Dirichlet BC for pressure on outflow. In contrast to variable viscosity and density, effect of viscous heating do not influence studied regimes significantly, but shows the accuracy of spectral/hp element approximation. Comparison with experimental data demonstrates influence of particular terms in the model using measurable quantities, e.g. Strouhal number or Nusselt number.

*e-mail: jpech@it.cas.cz

2 Navier-Stokes-Fourier system

Dimensionless system of equations representing flow of a heated fluid, which is supposed to be Newtonian, calorically perfect and obeying Fourier law, is often called the Navier-Stokes-Fourier system. In 2D, the unknowns are velocity $\mathbf{v} = (u, v)^{\mathrm{T}}$, pressure p and temperature T

$$\rho\left(\frac{\partial \mathbf{v}}{\partial t} + \mathbf{v}\cdot\nabla\mathbf{v}\right) = -\nabla p + \frac{1}{\mathrm{Re}}\nabla\cdot(2\mu\mathbb{S}) + \frac{1}{\mathrm{Fr}^2}\rho\mathbf{g} \tag{1a}$$

$$\frac{\partial \rho}{\partial t} + \nabla\cdot(\rho\mathbf{v}) = 0 \tag{1b}$$

$$\rho\left(\frac{\partial T}{\partial t} + \mathbf{v}\cdot\nabla T\right) = \frac{1}{\mathrm{Re}\,\mathrm{Pr}}\nabla\cdot(\kappa\nabla T) + \frac{\mathrm{Ec}}{\mathrm{Re}}2\mu\mathbb{S}:\mathbb{S}\,, \tag{1c}$$

where

$$\mathbb{S} = \mathbb{D} - \frac{1}{3}(\nabla\cdot\mathbf{v})\,\mathbb{I} \tag{2}$$

is related to the deviatoric part of the stress tensor (pure shear stress) and $\mathbb{D} = \frac{1}{2}\left[\nabla\mathbf{v} + (\nabla\mathbf{v})^{\mathrm{T}}\right]$. Term

$$\mathbb{S}:\mathbb{S} = \mathbb{D}:\mathbb{D} - \frac{1}{3}(\nabla\cdot\mathbf{v})^2 \tag{3}$$

is related to the effect of viscous heating. We do not impose any a priori restrictions to form of the temperature dependencies $\mu(T)$, $\kappa(T)$ and $\rho(T)$. Note, that this

Table 1. Definitions of nondimensional numbers used in system (1). Note, that the Eckert number in this form belongs to temperature normalised by value T^+_∞ instead of widely used characteristic temperature difference ΔT^+. L^+ is a characteristic length, c^+_p specific heat at constant pressure.

Name	Symbol	Definition
Eckert	Ec	$\frac{\lvert\mathbf{v}^+_\infty\rvert^2}{c^+_{p_\infty} T^+_\infty}$
Froude	Fr	$\frac{\lvert\mathbf{v}^+_\infty\rvert}{\sqrt{g^+_\infty L^+}}$
Prandtl	Pr	$\frac{c^+_{p_\infty}\mu^+_\infty}{\kappa^+_\infty}$
Reynolds	Re	$\frac{L^+\lvert\mathbf{v}^+_\infty\rvert\rho^+}{\mu^+_\infty}$
Richardson	Ri	$\frac{\Delta\rho^+ g^+ L^+}{\rho^+_\infty\lvert\mathbf{v}^+_\infty\rvert^2}$

formulation avoids the Boussinesque approximation of buoyancy, since the gravitational action (**g** is a unit vector oposite to gravitational force) to momentum balance comes purely from density variation. This approach is advantageous, because it avoids specification of the thermal expansion coefficient, what is the case of Boussinesque's model. The volumetric term $\rho\mathbf{g}/\mathrm{Fr}^2$ in this form brings two effects to the solution. Beside of buoyancy it includes model of hydrostatic pressure gradient. It might be advantageous to leave only the buoyancy what follows by subtraction of some, e.g. farfield[1], state from (1a). The volumetric term in (1a) then takes form

$$\frac{1}{\mathrm{Fr}^2}(\rho - 1)\mathbf{g} \tag{4}$$

and allow comparison with the results achieved with Boussinesque approximation through general form of the Richardson number since $(\rho - 1) = (\rho^+ - \rho^+_\infty)/\rho^+_\infty \approx \beta\Delta T$ (c.f. table 1, where dimensionless numbers are summarized).

Unless we consider only flow of air in this work, energy equation (1c) has the same structure for both the gases and liquids with the minor change, that specific heat at constant pressure c^+_p is replaced by c^+_V (specific heat at constant volume), c.f. redefinition of Pr by substituting $c_p \to c_V$.

3 Numerical method

3.1 Spectral/hp element method

The spectral/hp element method was chosen for approximation of functions in spatial coordinates. It combines decomposition of the computational domain Ω to elements Ω_e, $\Omega = \cup_{e=1}^{E}\Omega_e$, with high degree approximation on every element. Consequently, it provides high-order accuracy

[1]We denote farfield/reference values by subscript ∞ and quantities with physical units are denoted by '+' in superscript.

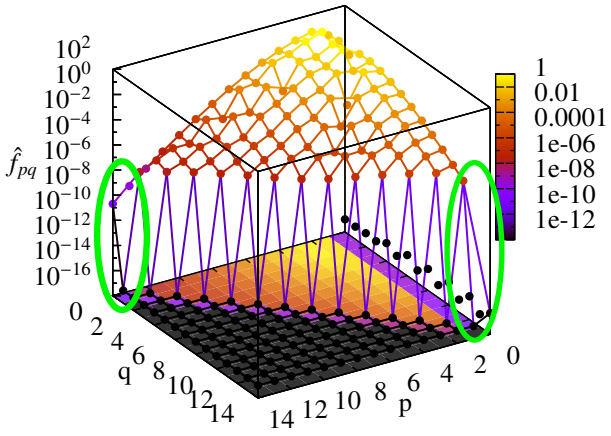

Fig. 1. Example of decaying spectra on a single triangular element for 2D polynomial expansion of degree $N = 14$. Spectral coefficients $\hat{f}_{pq}$ are only those with index $p+q <= N$ in the graph. Green ellipses show the maximal degree coefficients whose sum provides heuristical error estimate. For this case, one can conclude, that the spatial approximation *is not better than* 10^{-8}.

together with geometrical flexibility. It can be viewed as a generalisation of global, $E = 1$, spectral methods, which follows C^0 continuity among elements and finally coincides with hp-finite elements. The reason for choosing this method is in efficient achievement of high-order approximation, which significantly suppress numerical diffusion and dispersion, so the influence of particular terms of the equation system may be compared in the simulations. Other advantages of the method are in lowering the number of degrees of freedom in the algebraic system or providing an instant insight to estimates of error ([2]). Mentioned estimate of discretisation error comes from insight to a single-element spectra of expansion coefficients $\hat{f}_{pq}$, representing a function f

$$f(x, y) = \sum_{p,q=0}^{N} \hat{f}_{pq}\phi_p(x)\phi_{pq}(y) \tag{5}$$

as expanded over a basis $\mathcal{B}_N = \{\phi_{pq}\}^N_{p,q=0}$, which is in our case of polynomial type and has hierarchical structure, $\mathcal{B}_N \subset \mathcal{B}_{N+1}$(notation in (5) is for tensor-product type basis over triangles, for details see e.g. [3]). Exponentially converging spectra for a single triangular element is shown in Figure 1. An open source library Nektar++ [1] of version 3.3.0 with own substantial changes was used as a basis for implementation of the solver.

3.2 Discretisation in time

Computational scheme for system (1) combines multiple techniques. It is basically derived from solver for strictly incompressible, $\nabla \cdot \mathbf{v} = 0$, flow model [4]. It may be seen as a velocity-correction semi-implicit (IMEX) scheme

Table 2. Coefficients of IMEX schemes up to order 3.

Q	γ	α_0	α_1	α_2	β_0	β_1	β_2
1	1	1	-	-	1	-	-
2	3/2	2	−1/2	-	2	−1	-
3	11/6	3	−3/2	1/3	3	−3	1

with a high-order approximation of Neumann type pressure boundary condition (HOPBC). However, multiple extensions of the scheme had to be performed.

The variable viscosity was implemented following approach mentioned in [5]. It is based on splitting the variable parameter, e.g. $\mu(T) = \bar{\mu}+\mu_s$, to constant-in-time part $\bar{\mu}$ and part variable both in time and space, $\mu_s = \mu_s(\mathbf{x}, t)$. This splitting impose a limit to amplitude of μ_s to ensure stability (see [5]), but it preserves structure of equations solved in the scheme. Similar approach was used for splitting the variable thermal conductivity in the energy balance, as described in [6]. Temperature-dependent density $\rho(T)$ in both the momentum and energy balance was implemented following approach proposed in [7], where this variable property was only in momentum equation. The most significant feature of proposed scheme lies in non-trivial velocity divergence, which emerges as a consequence of thermal expansion of the heated material. The detail description of discretisation to the full system, which is beyond scope of this paper, is prepared to be published. Here, we will only sketch the key points of the method.

The scheme is based on approximation of the time derivatives by *Backward Difference Formula* of order Q

$$\frac{\partial f}{\partial t} \approx \frac{\gamma f_{n+1} - \sum_{q=0}^{Q-1} \alpha_q f_{n-q}}{\Delta t}, \tag{6}$$

where f represents u, v, T or ρ. Δt denotes discrete time step, γ and $\{\alpha_q\}_{q=0}^{Q-1}$ are coefficients of the BDF formula (see table 2) and $f_n = f(t_n)$ is the function value at time $t_n = t_0 + n\Delta t$.

We denote

$$[f]^* = \sum_{q=0}^{Q-1} \beta_q f_{n-q} \tag{7}$$

the Q-th order extrapolation consistent to chosen BDF formula. The scheme follows these steps:

1. solve Pressure-Poisson equation, which is derived from application of divergence operator to (1a)

$$\begin{aligned}\nabla^2 p = {} & \frac{\gamma}{\Delta t}\left(\left[\frac{\partial \rho}{\partial t}\right]^{**}\right) \\ & + \nabla\cdot\Big\{\frac{\gamma}{\Delta t}[\rho]^*\hat{\mathbf{v}} \\ & \quad + \frac{1}{\mathrm{Re}}\left[\nabla\mu\cdot\left(\nabla\mathbf{v} + (\nabla\mathbf{v})^{\mathrm{T}}\right) - \nabla\mu\cdot(\nabla\times\nabla\times\mathbf{v})\right]^* \\ & \quad + \frac{1}{\mathrm{Re}}\left(-\frac{2}{3}[\nabla\mu]^*\langle\nabla\cdot\mathbf{v}\rangle + \frac{4}{3}[\mu]^*\nabla\langle\nabla\cdot\mathbf{v}\rangle\right) \\ & \quad + \frac{1}{\mathrm{Fr}^2}[\rho]^*\mathbf{g}\Big\},\end{aligned} \tag{8}$$

where $\hat{\mathbf{v}} = \sum_{q=0}^{Q} \alpha_q \mathbf{v}_{n-q} - \Delta t\,[\mathbf{v}\cdot\nabla\mathbf{v}]^*$, $[\cdot]^{**}$ denotes extrapolation of time derivative approximated from BDF formula (6) and we used $\nabla\cdot(\rho\mathbf{v}) = -\partial\rho/\partial t$ from (1b). Forward estimate of divergence follows from extrapolation of (1b), since $\rho_n = \rho(T_n)$

$$\langle\nabla\cdot\mathbf{v}\rangle = \frac{1}{\rho^*}\left\{-[\mathbf{v}\cdot\nabla\rho]^* - \left[\frac{\partial\rho}{\partial t}\right]^{**}\right\} \tag{9}$$

Equation (8) is subject to the Dirichlet boundary condition or natural Neumann pressure boundary condition with high order extrapolation (HOPBC), which follows from projection of (1a) to boundary normal $\mathbf{n}$

$$\begin{aligned}\frac{\partial p}{\partial \mathbf{n}} = {} & \mathbf{n}\cdot\Big\{\Big[\quad -\rho\frac{\partial\mathbf{v}}{\partial t} - \rho\mathbf{v}\cdot\nabla\mathbf{v} \\ & \quad + \frac{1}{\mathrm{Re}}\left(-\mu\nabla\times\nabla\times\mathbf{v} + \nabla\mu\cdot\left[\nabla\mathbf{v} + (\nabla\mathbf{v})^{\mathrm{T}}\right]\right) \quad \Big]^* \\ & \quad + \frac{1}{\mathrm{Re}}\left(-\frac{2}{3}[\nabla\mu]^*\langle\nabla\cdot\mathbf{v}\rangle + \frac{4}{3}[\mu]^*\nabla\langle\nabla\cdot\mathbf{v}\rangle\right) \\ & \quad + \frac{1}{\mathrm{Fr}^2}[\rho]^*\mathbf{g}\Big\}\end{aligned} \tag{10}$$

2. The velocity-correction step then consists of solution to an elliptic problem

$$\begin{aligned}\nabla^2\mathbf{v}_{n+1} - \frac{\gamma}{\Delta t}\mathrm{Re}\mathbf{v}_{n+1} = {} & \\ & \Big\{ -\mathrm{Re}\frac{\gamma}{\Delta t}\hat{\mathbf{v}} \\ & \quad + \frac{1}{[\rho]^*}\Big[\mathrm{Re}(\nabla p_{n+1} - \mathbf{f}_{n+1}) \\ & \qquad - \left[\nabla\mu\cdot[\nabla\mathbf{v} + (\nabla\mathbf{v})^{\mathrm{T}}]\right]^* \\ & \qquad + \frac{2}{3}[\nabla\mu]^*\langle\nabla\cdot\mathbf{v}\rangle \\ & \qquad - \frac{1}{3}[\mu]^*\nabla\langle\nabla\cdot\mathbf{v}\rangle\Big] \quad \Big\} \\ & - (\nabla\langle\nabla\cdot\mathbf{v}\rangle - [\nabla\times\nabla\times\mathbf{v}]^*) \\ & \qquad \left[\left(\frac{1}{[\rho]^*}\right)_s [\mu]^* + [\mu]^*_s\right].\end{aligned} \tag{11}$$

Above equation has many terms on right-hand side, since the technique of splitting to constant and

variable-in-time part was done both to viscosity and density, c.f. [7].

3. Elliptic equation in similar form $(\nabla^2 - \lambda)T_{n+1} = \ldots$ is solved for temperature. Similarly to step 2), we split both $\kappa(T)$ and $\rho(T)$.

Unless the constant-in-time properties may be variable in space, the formulation is much more complicated and we set $\bar{\mu} = \bar{\kappa} = \bar{\rho} = 1$ for simplicity.

Convergence of the scheme was already verified on manufactured solutions, what is behind the scope of this contribution and is to be published together with more detail description of the scheme.

The buoyancy term in momentum equation (1a) is relatively easy to implement, but has substantial consequence in inclusion of complete model for natural convection. We consider $\mathbf{g}$ to be constant, and the buoyancy term is evaluated from extrapolated density in form including model of hydrostatic pressure gradient

$$\frac{1}{\mathrm{Fr}^2}[\rho]^*\mathbf{g}\,. \tag{12}$$

or without hydrostatics

$$\frac{1}{\mathrm{Fr}^2}([\rho]^* - 1)\mathbf{g} \tag{13}$$

accordingly to (4) as discussed in sec. 2.

The viscous heating, (3), in energy balance was included rather for completeness and testing. It is also evaluated as a pure extrapolation of data from previous time levels, while $\langle \nabla \cdot \mathbf{v} \rangle$ comes from (9).

4 Results

All computations presented concern air as the flowing medium. We use a power-law approximation for temperature dependencies of material properties μ, ρ and κ

$$f(T) = \frac{f^+_{ref}}{f^+_\infty}\left(\frac{T^+}{T^+_{ref}}\right)^{\omega_f} \tag{14}$$

(subscript "ref" denotes any virtual reference state following from the data-curve fit). Particular constants for $T^+_{ref} = 285\mathrm{K}$ are as follows

$$\begin{aligned} \mu^+_{ref} &= 1.78 \times 10^{-5}\,, \omega_\mu = 0.72 \\ \kappa^+_{ref} &= 0.025\,, \omega_\kappa = 0.84 \\ \rho^+_{ref} &= 1.239\,, \omega_\rho = -1.0013\,, \end{aligned} \tag{15}$$

derived from power-law regressions to data [8]. With the complete model (1) we study two cases, forced and natural convection.

4.1 Impact of variable material properties to vortex shedding frequency behind a heated cylinder

Flow around a cylinder is a widely used case for code testing and deep insight to flow physics for its simple geometry and sufficient available data. In this section, we compare our results from 2D simulations with experiments presented in [9] and also theoretically investigated in [10].

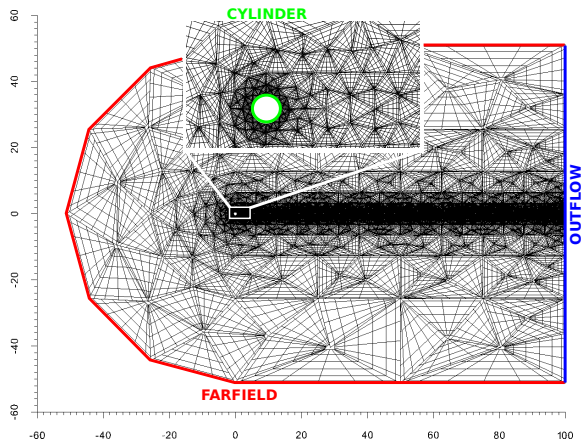

Fig. 2. Computational mesh with 2360 elements and domain boundary designation. Lines inside the domain connect quadrature points for degree 6 approximation inside triangular elements.

Data in [6] were computed with model including variable viscosity and thermal conductivity, while density was assumed constant and the velocity field was divergence free. Using the same computational mesh, boundary conditions and degree of polynomials $N = 6$ and other settings ($\Delta t = 0.001$), we recalculated the same situations. The boundary conditions are following (c.f. Figure 2):

- Farfield: $u = 1$, $v = 0$, $T = 1$, HOPBC
- Cylinder: $u = 0$, $v = 0$, $T = T^+_W/T^+_\infty$, HOPBC
- Outflow: $\partial u/\partial \mathbf{n} = 0$, $\partial v/\partial \mathbf{n} = 0$, $\partial T/\partial \mathbf{n} = 0$, $p = -g^+_\infty L^+ y/|\mathbf{v}^+_\infty|^2$

Pressure gradient set on the outflow boundary is consistent with used model of buoyancy, which includes the hydrostatic contribution. If buoyancy is modelled with (13), $p = 0$ on outflow is corresponding boundary condition. Constant fields with values $(u, v, T)^{\mathrm{T}} = (1, 0, 1)^{\mathrm{T}}$ were used as initial conditions.

High order approximation, polynomial of degree 15, was used also for representation of the deformed domain boundaries, the cylinder and upstream/inlet boundary, in the mesh. The second order scheme in time, $Q = 2$, was used as default.

Results from the new model and scheme are directly compared with experiment, [9], and previous numerical results in Figure 3. Reynolds numbers from [9] were recomputed for consistency with the relations describing material properties (15) (in [9] temperature dependence of kinematic viscosity was used in definition of Re, what is inconsistent with our model). It is worthy to emphasize, that model with constant density used in [6] strongly reflects the influence of temperature variation through variable viscosity and thermal conductivity, but is still insufficient as the results for highest temperature ratio ($\tilde{T} = T^+_W/T^+_\infty = 1.8$) coincide rather with different level of heating considered in experiment, compare coincidence of "emp. $\tilde{T} = 1.5$" and "cmp. [6] $\rho = \mathrm{const.}$". Finally, the current results coincide with experimental data more

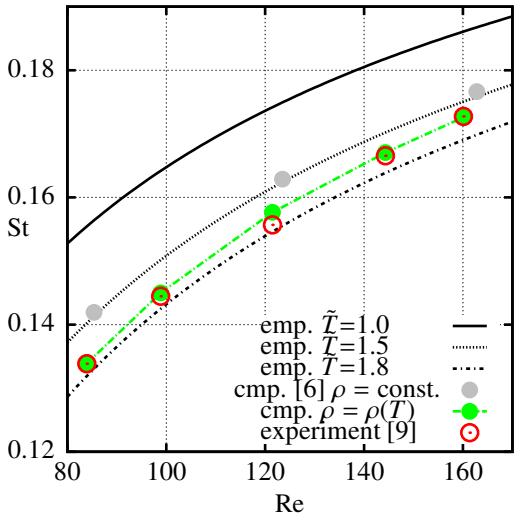

Fig. 3. Direct comparison of data from model proposed in [6] with current data (same setting of discretisation) and empirical formulas [10]. All computations "cmp." and experimental "exp." data belong to temperature ratio $\tilde{T} = T_W^+/T_\infty^+ = 1.8$.

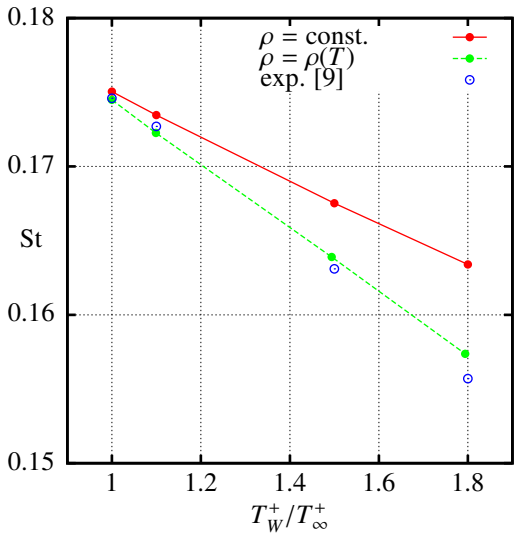

Fig. 4. Comparison of model with ρ = const. ([6]) and the current one with $\rho = \rho(T)$. The difference in dimensionless frequency of vortex shedding, St, is substantial. Computations followed Re from experiment, all being close to an average value Re ≈ 121.4.

accurately than empirically derived formula proposed in [10].

The difference between the models is even better visible in plot $\mathrm{St}(T_W^+/T_\infty^+)$ for fixed value of Re, see figure 4. From this comparison of current data and result from [6], we can separately discern influence of variable viscosity and variable density to the flow. Note, that only the value from experiment at $T_W^+/T_\infty^+ \approx 1.8$, used in Fig. 4, exhibit stronger deviation than other data also in Fig. 3.

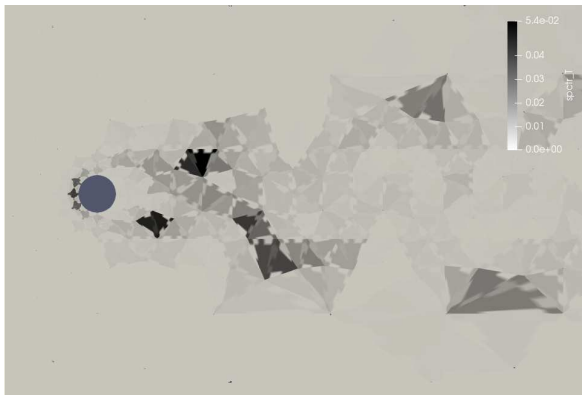

Fig. 5. Distribution of spatial error over the computational mesh. Values obtained as a sum of spectral coefficients belonging to highest degree boundary modes. Max value $\approx 5 \times 10^{-2}$.

The estimate of error in spatial discretisation as mentioned in sec. 3.1 is one of natural outputs from simulations in spectral/hp elements. Distribution of the error over the computational mesh, may be analysed at every timestep. Its evaluation is computationally cheap, since it is summation of only a few coefficients from the spectra of every element, c.f. figure 1. Figure 5 shows an example of this approach for a particular t_n on function representing temperature distribution in flow around heated cylinder. The error distribution changes as the function develops in time.

4.2 Natural convection

Flow motion induced by heating was investigated for validation of buoyancy model in presented scheme. Simple geometry of heated cylinder was chosen for comparison with previous data from literature. In [11], tabulated data are available. However, numerical method used in [11] differs substantially from the scheme proposed in sec. 3.2. Due to lack of data for this particular case in literature, we will compare results of model for steady incompressible constant-property flow with Boussinesque approximation for buoyancy with our model for evolutionary problem allowing non-homogeneous divergence, variable properties and without the Boussinesque's approximation.

Present simulation was performed with $\Delta t = 0.005$, polynomial degree $N = 24$ on mesh consisting of only 289 quadrilateral elements while the domain extent was $\Omega = [-500 : 500] \times [-500 : 500]$ for cylinder of diameter 1. Curve representing the cylinder was approximated by polynomial of degree 17. Domain dimensions were so large, that the buoyant disturbances travelling through the volume did not reach $\partial\Omega$ during whole time interval, $t \in [0 : 350]$. Therefore, the physical meaning of the solution was not strongly influenced by inaccuracy following from boundary conditions, which were as follows

- Inlet: $\partial u/\partial \mathbf{n} = 0$, $\partial u/\partial \mathbf{n} = 0$, $T = 1$, $p = 0$
- Sides: $u = 0$, $v = 0$, $T = 1$, HOPBC
- Cylinder: $u = 0$, $v = 0$, $T = T_W^+/T_\infty^+ = 1.05$, HOPBC

• Outflow: $\partial u/\partial \mathbf{n} = 0, \partial v/\partial \mathbf{n} = 0, \partial T/\partial \mathbf{n} = 0, p = 0$

Shape of the computational domain was similar to Fig. 2 with half-circle arc on inlet. Gravity action was in direction of domains axis of symmetry. Initial conditions were $(u, v, T)^{\mathrm{T}} = (0, 0, 1)^{\mathrm{T}}$. Used model of buoyancy was without the hydrostatic pressure gradient, (13).

Simulation was performed for three values of Rayleigh number, $\mathrm{Ra} = \mathrm{Ri}\,\mathrm{Pr}\,\mathrm{Re}^2$, $\mathrm{Ra} \in \{10^2, 10^3, 10^4\}$. Material parameters for air were used, the same as in the case of forced convection over heated cylinder as discussed in sec. 4.1. Some value of Re has to be defined to the solver, however it is unknown a priori. It follows from binding of Re and Fr through L^+ and $|\mathbf{v}_\infty^+|$ (see Table 1), that lower influence of viscous term implies lower influence of buoyant term for fixed Ra. Instability of the scheme occured for values $1/\mathrm{Fr}^2$ of order 10 if $\mathrm{Re} < 50$. All simulations run with $T \in [1 : 1.05]$ and their inputs were

• $\mathrm{Ra} = 10^2$: $\mathrm{Re} = 100$, $L^+ = 0.00475$, $|\mathbf{v}_\infty^+| = 0.3 \Rightarrow \dfrac{1}{\mathrm{Fr}^2} = 0.51$

• $\mathrm{Ra} = 10^3$: $\mathrm{Re} = 100$, $L^+ = 0.01$, $|\mathbf{v}_\infty^+| = 0.14 \Rightarrow \dfrac{1}{\mathrm{Fr}^2} = 5.1$

• $\mathrm{Ra} = 10^4$: $\mathrm{Re} = 300$, $L^+ = 0.02$, $|\mathbf{v}_\infty^+| = 0.196 \Rightarrow \dfrac{1}{\mathrm{Fr}^2} = 5.6$

Note, that above values of Re are parameters chosen only for proper definition of the solved problem and stability of computation and have to be recalculated using some well defined values from solution fields for full comparison with experiment.

Comparison of local Nusselt number, $\mathrm{Nu} = \mathbf{n} \cdot \nabla T$, over the cylinder surface is in figure 6 and difference between the results is well observable. Similar difference, especially in vicinity to cylinder surface can be seen also in comparison of experimental and numerical isotherms already in [11], fig. 7. Similar difference to Kuehn's data in local Nusselt number was reported in [12], where a fourth order approximation in space was used in computation of steady model. Work [12] does not contain tabulated data and we have to conclude with only this qualitative comment to comparison with our data.

To emphasize the novelty of our scheme, we show distribution of velocity divergence, result of thermal expansion of the heated air, see figure 7. The same figure contains detail of computational mesh in vicinity of the cylinder and presents also the spatial resolution of variable u. For this field, in vicinity of the cylinder, worst element spectrum is converged to values around 10^{-6} and in elements on cylinder boundary we observe even better resolution up to 10^{-12}, what coincides with round-off tolerance in the Nektar++ library.

In contrast to cited stationary models we observe flow instability in present results as shown in Fig. 4.2 for $\mathrm{Ra} = 10^3$ and 10^4. These figures belong to the same time-step ($t_n = 250$). Wake in Fig. 4.2-A shows a pair of strong vortices, which travel from the cylinder while the wake becomes unstable, what can be seen from variation of mean

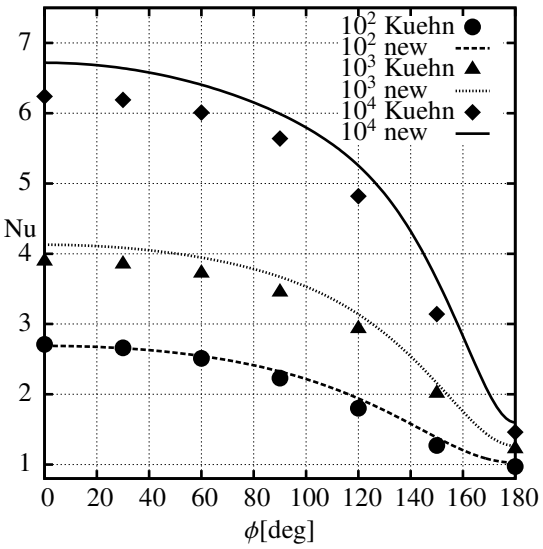

Fig. 6. Nusselt number distribution over cylinder in natural convection, comparison of data from [11] and the new scheme for $\mathrm{Ra} \in \{10^2, 10^3, 10^4\}$. Angle ϕ is measured from the lowest point of the cylinder.

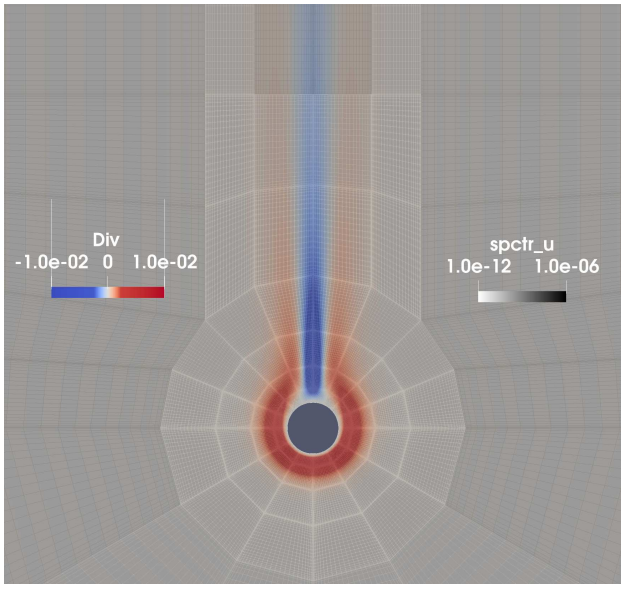

Fig. 7. Field of velocity divergence "Div" in natural convection problem with Ra = 1000. Spatial error estimate "spectr_T" for temperature field is projected onto the divergence field together with mesh grid, which belongs to approximation by polynomial of degree 24.

Nusselt number in Fig. 9. For $\mathrm{Ra} = 10^4$ we early observe development of instability and complicated vortex structures.

Obtained mean (integral) values of Nusselt numbers are

• $\mathrm{Ra} = 10^2$: $\mathrm{Nu}_{\mathrm{mean}} \approx 2.1$

• $\mathrm{Ra} = 10^3$: $\mathrm{Nu}_{\mathrm{mean}} \approx 3.3$

• $\mathrm{Ra} = 10^4$: $\mathrm{Nu}_{\mathrm{mean}} \approx 5.3$

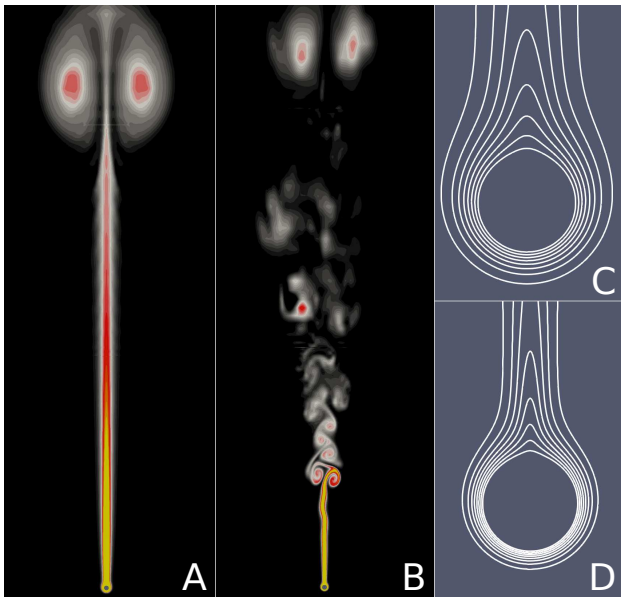

Fig. 8. Comparison of temperature fields for Ra = 10^3, (A and C), and Ra = 10^4, (B and D). 8 contours visible in the cylinder area (C, D) have regular spacing and cover range of temperature $T \in (1 : 1.05)$.

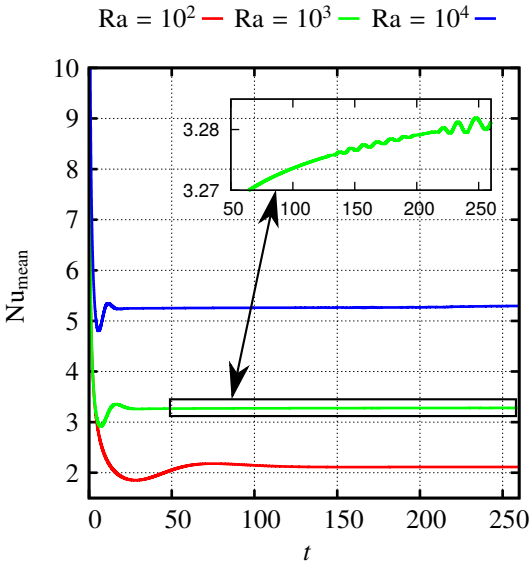

Fig. 9. Temporal evolution of mean Nusselt number $\mathrm{Nu}_{\mathrm{mean}}$ for various values of Ra. Rescaled detail for Ra = 10^3.

We emphasize that above values are approximative, since the non-stationary nature of the flow is reflected in this data evaluated from the boundary layer on the cylinder. Mentioned instability is shown in a detail view inside Fig. 9.

4.3 Viscous heating

Effect of viscous heating is negligible in both studied cases, but running the simulation of forced convection case with the full model and $T_W^+ = T_\infty^+$ returns the temperature field shown in figure 10. Negligible variation being under resolution of less accurate numerical approximations is here well recognized, for more, the resulting field is smooth, unless the viscous heating term is evaluated through spatial derivatives of the velocity field and includes also the square of $\langle \nabla \cdot \mathbf{v} \rangle$, which is purely extrapolated and may accumulate numerical error.

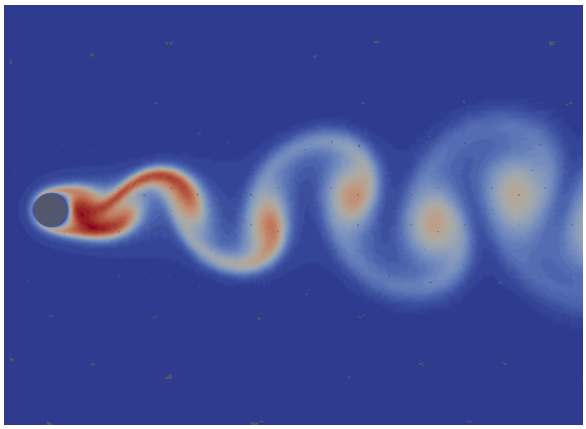

Fig. 10. Temperature field induced purely by viscous heating term (Re = 121.8, $T_W^+ = T_\infty^+$). Maximal variation of this normalized temperature is 3.8×10^{-6}.

5 Conclusion

Problem of cross-influence of heat and velocity field was studied in this work. Model for heated flow consisting of coupled system of momentum, mass and energy balance was formulated and appropriate numerical scheme was proposed. The system of equations is very general and similarities may be found also with turbulence models. Up to the authors knowledge, this is first implementation of this kind of models to spectral/hp methods. Field of numerical simulations of heated flows with variable material properties is not very wide and results found in literature seem to be mostly restrictions of the model and scheme presented in this contribution. Testing the convergence and rigorous description of the scheme is demanding and was left to specialized paper.

Performance of the scheme was tested on 2D simulations of evolutionary problems, forced convection over heated cylinder and natural convection induced by heating of the fluid on cylinder wall. Very good coincidence with experimental data [9] was achieved. Improvement of achieved Strouhal-Reynolds relationship for various temperatures of cylinder was recognized as substantial in comparison with previous model proposed in [6]. Current data very well coincide with experiments and uncover strong impact of both thermal expansion and change of viscosity to heated flow in regime of forced convection.

Numerical result achieving resolution to computer precision in cylinder area and boundary layer was achieved in problem of natural convection. It is observable from these results (e.g. figure 7), that the divergence of velocity induced by thermal expansion of the fluid reaches its maxima in certain distance from the heated surface. Di-

vergence distribution in the boundary layer will be one of the subject for future detail investigations, since its model inclusion represents one of the novelties of introduced numerical scheme. In comparison with previous data from literature, difference in distribution of local Nusselt number over cylinder surface was observed and should be confirmed by further detail comparison with experimental data.

In studied cases, good performance of spectral/hp element method was shown, both in sense of accuracy of spatial approximation and effectivity of the algorithm for evolutionary problems. Original strategy of error estimate in spatial approximation, following from insight to coefficient spectra, was outlined.

Acknowledgements. The author wishes to acknowledge the support of the Czech Academy of Sciences, project MSM100761901.

References

1. C. Cantwell, D. Moxey, A. Comerford, A. Bolis, G. Rocco, G. Mengaldo, D.D. Grazia, S. Yakovlev, J.E. Lombard, D. Ekelschot et al., Computer Physics Communications **192**, 205 (2015)
2. J. Pech, P. Louda, *Comparison of Finite Volume and Spectral/HP Methods on Navier - Stokes Equations for Unsteady Incompressible Flow*, in *Proceedings Topical Problems of Fluid Mechanics 2018* (2018), pp. 223–230
3. G. Karniadakis, S. Sherwin, *Spectral/hp Element Methods for Computational Fluid Dynamics: Second Edition*, Numerical Mathematics and Scientific Computation (OUP Oxford, 2005), ISBN 9780198528692
4. G.E. Karniadakis, M. Israeli, S.A. Orszag, Journal of Computational Physics **97**, 414 (1991)
5. G.S. Karamanos, S. Sherwin, Applied Numerical Mathematics **33**, 455 (2000)
6. Pech, J., EPJ Web of Conferences **114**, 02089 (2016)
7. J. Pech, *Scheme for evolutionary Navier-Stokes-Fourier system with temperature dependent material properties based on spectral/hp elements*, in *Lect. Notes Comput. Sci. Eng.* (In print)
8. B. Gebhart, *Heat Conduction and Mass Diffusion*, McGraw-Hill series in mechanical engineering (McGraw-Hill, 1993), ISBN 9780071125147
9. A.B. Wang, Z. Trávníček, K.C. Chia, Physics of Fluids **12**, 1401 (2000), https://doi.org/10.1063/1.870391
10. F. Maršík, Z. Trávníček, R.H. Yen, A.B. Wang, in *Proceedings of CHT-08* (DOI:10.1615/ICHMT.2008.CHT.210)
11. T. Kuehn, R. Goldstein, International Journal of Heat and Mass Transfer **23**, 971 (1980)
12. T.V.S. Sekhar, B.H.S. Raju, International Journal of Physical and Mathematical Sciences **6**, 1032 (2012)